

COMPARISON BETWEEN BRIGHTNESS TEMPERATURE AND REFLECTIVITY TO THICKNESS OF SEA-ICE

K. Naoki^{a,*}, J. Ukita^b, F. Nishio^c, K. Nakamura^d, M. Nakayama^e

^a EORC, JAXA 2-1-1, Sengen, Tsukuba, Ibaraki - naoki.kazuhiro@jaxa.jp

^b Faculty of Science, Niigata University, 8050 Igarashininomachi, Nishiku, Niigata - jukita@env.sc.niigata-u.ac.jp

^c CEReS, Chiba University, 1-33 Yayoicho, Inage, Chiba - fnishio@faculty.chiba-u.jp

^d GEO Grid Research Group Information Technology Research Institute, AIST, 1-1-1 Umezono, Tsukuba, Ibaraki - nakamura-kazuki@aist.go.jp

^e Department of Academic Coaching Studies, Hokusyo University 23 Bunkyo-dai, Ebetsu, Hokkaido - nakayama@hokusho-u.ac.jp

Commission VIII, WG VIII /10

KEY WORDS: Sea-ice, Brightness temperature, thickness, reflectance, AMSR-E

ABSTRACT:

Sea ice is an essential component of the global climate system since it influences and is influenced by changes and variations in the global energy balance and water cycle. In the context of decreasing SIE over the Arctic and an increasing area covered by the seasonal ice, spatial and temporal variations in thin ice especially its thickness are important research questions. The brightness temperature characteristic to thickness is important because it estimates from the brightness temperature. And the verification of the estimated result is also important. However, the observation of thin sea ice is difficult. Therefore, the comparison with other data is important. The reflectivity of visible and near-infrared has a low characteristic in the thin sea ice area. The purpose of this study clarified the brightness temperature characteristic of sea ice, and compared the relations between reflectivity and the brightness temperature of the sea ice. The compared data is a brightness temperature from AMSR-E and reflectivity from MODIS. The analysis converted the projection of both data into the same polar stereographic. And, the clear regions were chosen from the cloud flag and compared. The analytical result on January 15, 2003 is reported. The pixel of reflectivity 0.2-0.3 of MODIS band 1 was distributed about 80% in brightness temperature of 185-190K. And the pixel of reflectivity 0.2 of MODIS band 2 was distributed about 80% in same brightness temperature. On the other hand, the pixel of reflectivity 0.7 of MODIS band 1 was distributed about 65% in brightness temperature of 240-245K. And the pixel of reflectivity 0.7-0.8 of MODIS band 2 was distributed about 80% in same brightness temperature. The reflectance of visible and near-infrared are low in thin sea-ice. The reflectivity of bands 1 and 2 has concentrated on 0.3 or less in low brightness temperature area. Therefore, it seems very possible that this area is thin region. In general the visible reflectance of the snow is 0.8 or more and near-infrared reflectance is about 0.6 different according to the grain size. The reflectivity of band1 and band2 concentrated on a high value in high brightness temperature area. The snow exists on the sea-ice, and it suggests the existence of thick sea ice in this area. Therefore, the brightness temperature of 18Ghz is low in thin ice, and thought to rise while growing up. Therefore, the brightness temperature of 18Ghz will be low in thin condition, and rise while growing up.

1. INTRODUCTION

The seasonal sea-ice accounts for a significant portion of the sea-ice cover. This implies that globally large part of sea-ice undergoes the stage of thin ice at least one point within a seasonal cycle. In a freezing condition thin-ice is associated with the formation of sea-ice, which is closely linked to the formation of dense water in sub-polar and polar oceans [Vinje et al, 2002; Tamura et al., 2008]. The amount of heat flux through sea-ice of thickness <0.5 m is 1 or 2 orders of magnitude higher than that through thicker ice [Maykut, 1978]. Anomalous sea-ice cover and resulting heat fluxes could influence large-scale atmospheric circulation [Honda et al., 1999]. In the context above accurate information on temporal and spatial distributions of thin ice is of significant importance to regional- and basin-scale heat budgets and atmosphere-ocean interaction.

For sea-ice of a thickness <0.3 m that includes nilas (thickness <0.1 m) and young ice (0.1-0.3 m of thickness) thickness has been estimated using various remote sensing methods. Of which passive microwave radiometry is becoming a first choice in many applications for its relative robustness under different weather conditions. Although exact methods vary among investigators [Steffen, 1991; Cavalieri,1994; Drucker et al., 2003; Martin et al., 2004; Tamura et al., 2008; Nishio et al., 2009] all thickness estimates using passive microwave radiometry are based on a presumed sensitivity of brightness temperature to sea-ice thickness, which has been identified for a thickness less than about 0.2-0.3 m. In some cases emissivity (a ratio of brightness temperature to physical temperature) instead of brightness temperature was used. An underlying process is that passive microwave radiometric signals contain indirect information on ice thickness through the dependence of dielectric properties on brine [Naoki et al., 2008 and see

* Corresponding author. This is useful to know for communication with the appropriate person in cases with more than one author.

references therein]. Within a range of frequencies and polarizations the observed thickness-brightness temperature relationship is more pronounced at lower frequencies (e.g. 18GHz) and horizontal polarization. Besides passive microwave other remote sensing techniques such as laser and radar altimetry and SAR are available to estimate sea-ice thickness. The altimetry is based on a direct measurement and more effective for thicker ice while the latter is still difficult to implement. Another remote sensing method to estimate thickness for thin sea-ice is through optical property. Within the thin category sea-ice is optically more transparent than the thicker counterpart [Perovich, 1990, 1991; Allison et al., 1993]. Massom and Comiso [1994] studied detailed dependence of visible and infrared albedos on different ice thickness and surface conditions using Advanced Very High Resolution Radiometer (AVHRR) satellite images. Based on a field study in the Arctic Ocean Ehn et al. [2007] also reported a relationship between spectral albedo and a thickness for a range of wavelength from the UV to infra-red (see their figures 10 and 11). However there has been no previous attempt to systematically compare albedo and reflectance with brightness temperature or with emissivity based on satellite observations. With this background the purpose of this study is to extend the previous results so as to investigate the relationship between brightness temperature/emissivity and visible and infra-red reflectance, in particular using satellite observations over the Sea of Okhotsk. By setting the Sea of Okhotsk as the target area, which is located in southerly latitudes approximately between 45 to 60 degrees, we are able to minimize possible influences of a low zenith angle of the sun on optical measurements. One of the remaining difficulties in the estimation of ice thickness using satellite passive microwave radiometry is our limited capability in validation. The method has been validated against thickness measurements, which are very rare due to a difficulty in measuring a thickness for thin ice. The existing measurements are also localized either by an upper-looking sonar [e.g. Drucker et al., 2003; Tamura et al., 2007] or by in situ [Naoki et al., 2008]. In comparison satellite data represent an averaged view over a much larger area. Given a trade off existing between optical and satellite passive microwave observations in terms of resolution and all-weather capability, a better knowledge of the relationship between reflectance and brightness temperature/emissivity on thin sea-ice is expected to provide valuable information for validating thin-ice algorithms.

2. DATA AND METHOD

For satellite data we make a use of reflectance and brightness temperature from the same satellite "AQUA". This is to make geo-reference and synchronization as precise as possible. Moderate-Resolution Image Spectroradiometer (MODIS) on board AQUA provides radiometric measurements in 36 spectral bands ranging in wavelength from 0.4 μm to 14.4 μm . Of which this study uses the Level 1B products of Band 1 (0.620–0.670 μm) and 2 (0.841–0.876 μm), whose nominal resolution was 250m.

Another sensor onboard AQUA is Advanced Microwave Scanning Radiometer (AMSR-E), which measures microwave emission of Earth's surface at 7 frequencies (6.925, 10.65, 18.7, 23.8, 36.5 and 89GHz as center frequencies) and at vertical and horizontal polarizations. It is a conically scanning system with a swath width of about 1445 km with the incidence angel fixed at about 55 deg. The instantaneous field of view of this sensor is 74 by 43 km at 6 GHz and decreasing with frequency to about 6

by 4 km at 89 GHz. The frequencies that have been used for sea-ice thickness estimation vary among investigators. As pointed out in Naoki et al. [2008] there are both observational and theoretical grounds that the sensitivity of brightness temperature to thickness is higher for lower frequencies. There is however a tradeoff between this sensitivity and spatial resolution. Furthermore, the high frequency such as 89 GHz suffers from a bias due to the presence of water vapor.

Considering such factors we choose 18GHz that provides a ground resolution of about 27 by 16 km.

Both reflectance and brightness temperature measurements from satellite correspond to "averaged view" over a large footprint especially for AMSR-E. Since sea ice concentration for such a large area is less than 100% it is necessary to make a correction for open water within a grid. There are two algorithms for the estimation of sea ice concentration, the enhanced NASA Team 2 and bootstrap algorithms [Markus and Cavalieri, 2000; Comiso, 2003]. The former uses gradient ratio (GR) and polarization ratio (PR) based on the brightness temperatures of 18GHz and 36GHz for both polarizations. In comparison, the latter algorithm is based on the brightness temperatures of both polarizations at 36GHz and vertical polarization at 18GHz. Hence, the combined use of the bootstrap algorithm and horizontal polarization at 18GHz for estimating thickness constitutes a complimentary set of frequencies and polarization. This study also uses sea ice surface temperature data calculated from brightness temperature at 6 GHz [Comiso et al., 2003]. The AMSR-E brightness temperature, sea ice concentration and sea ice surface temperature data were all acquired from the download site at National Snow and Ice Data Center (NSIDC).

Prior to the analysis MODIS data were corrected for the zenith angle of the sun. Then MODIS data, surface temperature and sea ice concentration were all projected onto the same polar stereographic coordinates as the one used by the AMSR-E. Next using the cloud mask 17 MODIS scenes in relatively cloud-free conditions were identified spanning the period of 2003 to 2007 (see Fig 1b and Table 1). For each grid of those scenes brightness temperature of sea-ice corrected for sea ice concentration was calculated assuming 0.332 as the emissivity of the sea water (Eppler, 1992) and the freezing temperature 271.35K.

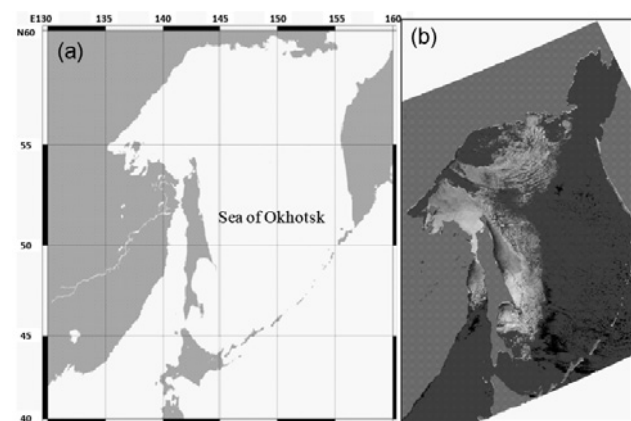


Figure 1. (a)Geographic location of Sea of Okhotsk (b) MODIS Band1 reflectance image on JAN 17, 2003.

3. RESULTS

3.1 Reflectance, brightness temperature and emissivity

Figure 1a shows the study region, the Sea of Okhotsk, in which sea-ice has been extensively investigated especially in conjunction with polynyas and the formation of North Pacific mode water [see references in Nihashi et al., 2009]. Figure 1b presents a sea-ice cover of the Okhotsk Sea on January 17, 2003 with the largest clear-sky area among those 17 MODIS scenes. For this image we identified 7154913 pixels for MODIS and corresponding 2851 pixels for AMSR-E. Figure 2a and 2b present the relationship of brightness temperature and reflectance for MODIS Band 1 and 2, respectively. There is a positive relationship between the brightness temperature and reflectance for both bands. For example, the averages of reflectance were 0.24, 0.41 and 0.55 for the brightness temperature ranges of 175-180 K, 210-215 K and 235-240 K. Similarly for Band 2 the averages of reflectance were 0.18, 0.38 for the same brightness temperature intervals.

The above results strongly support that both reflectance and brightness temperature are sensitive to a thickness for thin ice with a close to linear relationship. What is remarkable is that those two measurements reflect physically different processes. They are attributed to optical property and dielectric property associated with brine, respectively. However, those results are likely biased by differences in surface temperatures. For example, a single MODIS image represents a significant North-South extension, which corresponds to a large air-temperature gradient within the Okhotsk Sea (see figure 1 of Nihashi et al., 2009). In order to correct for this bias we calculated emissivity (brightness temperature divided by surface physical temperature) for each AMSR-E grid (Figure 2c and 2d). Note that there is a marked relationship between emissivity and reflectance for both bands. Furthermore, the relationship is close to be linear for this range of emissivity and reflectance.

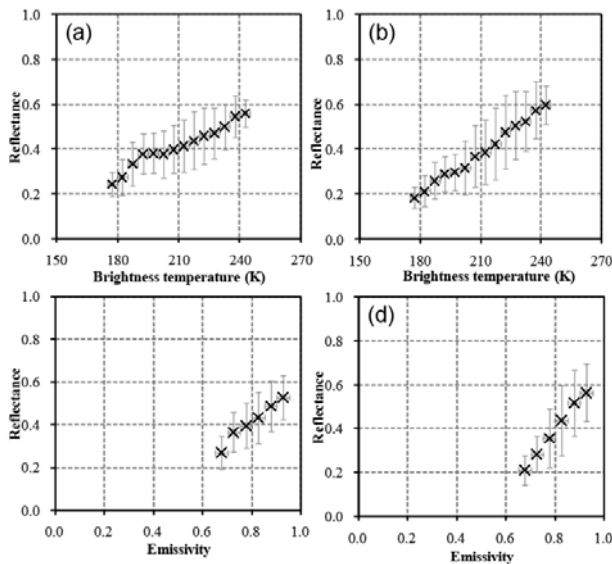


Figure2. Comparison AMSR-E and MODIS
 (a) Brightness temperature of sea ice vs. reflectance (Band1).
 (b) Brightness temperature of sea ice vs. reflectance (Band2).
 (c) Emissivity of sea ice vs. Reflectance (Band1). (d) Emissivity of sea ice vs. Reflectance (Band2).

3.2 Thickness estimate

In all likelihood brightness temperature is a proxy for a thickness for thin sea-ice. As was seen for a large area such as the Okhotsk Sea with a significant surface temperature gradient, emissivity which by definition includes a surface temperature correction is likely a better parameter for ice thickness. For the Okhotsk Sea our previous study found thresholds in emissivity for different thickness categories, $\epsilon < 0.76$ for an ice thickness $< 0.1m$ and < 0.84 for a thickness $> 0.2m$. Figure 3a and 3b present histograms of reflectance for the grids with reflectance of 0.755 to 0.765 for Band 1 and 2, respectively. In comparison, Figure 3c and 3d plot the same for the grids with reflectance of 0.835 to 0.845 for Band 1 and 2. Note that by utilizing all 17 MODIS scenes the number of samples was rather large, e.g. $n=4860$ and $n=19236$ for two thresholds values. For Band 1 (visible) the averages in reflectance increase from 0.42 to 0.56 with the standard deviations of 0.08 and 0.10 respectively. It is also noted that all distributions in Figure 3 are highly skewed with long tails to lower values in emissivity. These distributions, if they present real characteristics of the relationship between emissivity and reflectance, can be used to provide error estimates on a relationship between them by a means of Monte Carlo simulation.

Even though we have corrected possible biases due to surface temperature gradient there still remains another source of bias. That is when emissivity is used for classifying ice thickness surface temperature must be corrected for sea ice concentration. Unfortunately surface temperature data which we used were not corrected for sea ice concentration.

In order to see how those two sources of biases may contribute to emissivity we select two small areas within a single MODIS scene where the two areas are as close to be cloud-free and to meet 100% sea ice concentration as possible. In addition the two areas are different thickness categories defined by the above thresholds in emissivity. For those two areas the average of Band 1 reflectance for the area corresponding to the thinnest category ($\epsilon < 0.75$) is 0.39 with 0.03 of standard deviation. The average increases to 0.56 while the standard deviation remains at 0.02. These standard deviations are significantly lower compared with the standard deviations of reflectance in Figure

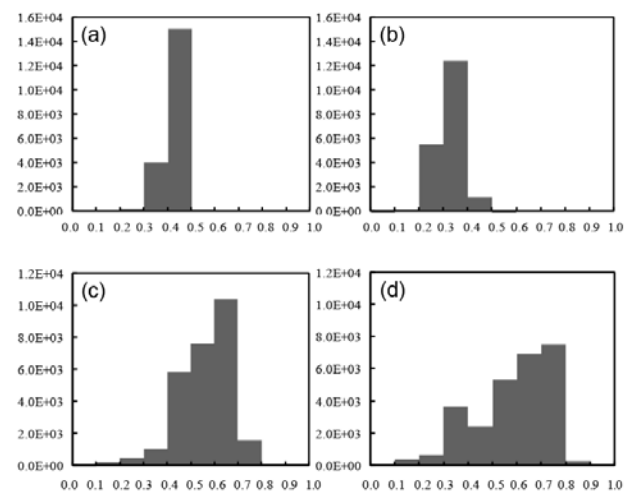


Figure3. Distribution of reflectance of threshold at emissivity
 (a) Distribution of Band1 on threshold 0.76. (b) Distribution of Band2 on threshold 0.76. (c) Distribution of Band1 on threshold 0.84. (d) Distribution of Band1 on threshold 0.84.

3, e.g. at least by a factor of 4. The brightness temperature used to estimate is strongly received salinity and the temperature influence on the ice surface in thin sea ice. The reflectance band1 and band2 changes because solar radiation is scattered and reflecting by a sea ice surface and an internal bubble, brine, etc. Both are mutually observing ice by an independent process. It is thought that such both having shown a good agreement in the comparative result estimated thickness from this method by high accuracy.

4. SUMMARY

This study aimed to estimate the thickness of thin sea ice from the brightness temperature observed with AMSR-E and developed the technique.

It has been understood that the temperature of 18GHz observed in the satellite can presume thickness from the comparison with the reflectance of visible and infrared rays. The brightness temperature of 18GHz H-pol from AMSR-E can estimate thickness that it compared with the reflectance MODIS band1 band2. The thickness of the sea ice estimated and used emissivity from the brightness temperature of 18GHz H-pol and the surface temperature. Both are observing the sea ice by a different respectively process.

The estimated result and reflectance showed a good agreement from the comparison result. This method estimate thickness from the 18GHz H-pol brightness temperature. Therefore, the brightness temperature of the sea ice can be estimated without receiving the influence of the sea ice concentration by select the sea ice concentration product. And, it is possible to apply to not only SSM/I but also SMMR that has been observed since 1978, and the possibility that the change of the sea ice for over 30 years including thickness can be clarified is high

References

Allison, I., R. E. Brandt, and S. G. Warren. 1993. East Antarctic sea ice: albedo, thickness distribution and snow cover. *J. Geophys. Res.*, **98**, 12,417-12,429.

Cavalieri, D. J. 1994. A microwave technique for mapping thin sea ice. *J. Geophys. Res.*, **99**(C6): 12,561-12,572.

Comiso, J. C., D.J. Cavalieri and T. Markus. 2003. Sea ice concentration, ice temperature, and snow depth using AMSR-E data. *IEEE Trans. Geosci. Remote Sens.*, **41**, 243-252.

Drucker, R., S. Martin, and R. Moritz. 2003. Observations of ice thickness and frazil ice in the St. Lawrence Island polynya from satellite imagery, upward looking sonar, and salinity/temperature moorings. *J. Geophys. Res.*, **108**, doi:10.1029/2001JC001213.

Eppler, D. and 14 other co-authors. 1992. Passive microwave signature of sea ice, Chap 4 in *Microwave Remote Sensing of Sea Ice*, Geophys. Monogr. 68, AGU, Washington D. C., 47-71.

Hall, D. K., Key, J. R., Casey, K. A., Riggs, G. A., D. J. Cavalieri. 2004. Sea Ice Surface Temperature Product From MODIS. *IEEE Trans. Geosci. Remote Sens.*, **42**(5), 1076-1087.

Markus, T., and D.J. Cavalieri. 2009. The AMSR-E NT2 Sea Ice concentration Algorithm: its Basis and Implementation. *Journal of the Remote Sensing Society of Japan*, **29**(1), 216-225.

Martin, S., R. Drucker, R. Kwok, and B. Holt. 2004. Estimation of the thin ice thickness and heat flux for the Chukchi Sea Alaskan coast polynya from Special Sensor Microwave/Imager data, 1990-2001. *J. Geophys. Res.*, **109**, doi:10.1029/2004JC002428.

Massom, R., and J. C. Comiso. 1994. The classification of Arctic Sea ice types and the determination of surface temperature using advanced very high resolution radiometer data. *J. Geophys. Res.*, **99** (C3), 5201-5218.

Maykut, G. 1978. Energy exchange over young sea ice in the central Arctic. *J. Geophys. Res.*, **83**, 3646-3658.

Naoki, K., J. Ukita, F. Nishio, M. Nakayama, and Al Gasiewski. 2008. Characteristic on Brightness Temperature of Thin Sea-Ice in the southern Sea of Okhotsk. *J. Geophys. Res.*, **113**, C02S16, doi:10.1029/2007JC004270.

Nihashi, S., K. I. Ohshima, T. Tamura, Y. Fukamachi, and S. Saitoh. 2009. Thickness and production of sea ice in the Okhotsk Sea coastal polynyas from AMSR-E. *J. Geophys. Res.*, **114**, doi:10.1029/2008JC005222.

Perovich, D.K. 1990. Theoretical Estimates of Light Reflection and Transmission by Spatially Complex and Temporally Varying Sea Ice Covers. *J. Geophys. Res.*, **95**(C6), 9557-9567.

Perovich, D. K. 1991. Seasonal changes in sea ice optical properties during fall freezeup. *Cold Region Science and Technology*, **19**, 261-273.

Piepmeyer, J.R., and Gasiewski, A.J. 1996. Polarimetric Scanning Radiometer for airborne microwave imaging studies, *Proceedings of the 1996 International Geoscience and Remote Sensing Symposium*, 1688-1691.

Honda, M., K. Yamazaki, H. Nakamura, and K. Takeuchi. 1999. Dynamic and thermodynamic characteristics of atmospheric response to anomalous sea-ice extent in the Sea of Okhotsk. *J. Clim.*, **13**, 617-633.

Steffen, K. 1991. Energy flux density estimation over sea ice based on satellite passive microwave measurements. *Ann. Glaciol.*, **15**, 178-183.

Tamura, T, K. I. Ohshima, T. Markus, D. J. Cavalieri, S. Nihashi, and N. Hirasawa. 2007. Estimation of thin ice thickness and detection of fast ice from SSM/I data in the Antarctic Ocean. *Journal of Atmospheric and Oceanic Technology*, **24**, 1757-1772.

Tamura, T., K. I. Ohshima, and S. Nihashi. 2008. Mapping of sea ice production for Antarctic coastal polynyas. *Geophys. Res. Lett.*, **35**, L07606, doi:10.1029/2007GL032903.

Vinje, T., T. Loyning, I.V. Polyakov. 2002. Effects of melting and freezing in the Greenland Sea, *Geophys. Res. Lett.*, **29**, 2129, doi:1029/ 2002GL015326